Structures of Perfringolysin O Suggest a Pathway for Activation of Cholesterol-dependent Cytolysins

ARTICLE *in* JOURNAL OF MOLECULAR BIOLOGY · MAY 2007

Impact Factor: 4.33 · DOI: 10.1016/j.jmb.2007.01.042 · Source: PubMed

6 AUTHORS, INCLUDING:

Susanne C Feil
Saint Vincent's Institute
37 PUBLICATIONS **2,107** CITATIONS
SEE PROFILE

Craig James Morton
St. Vincent's Institute
74 PUBLICATIONS **2,783** CITATIONS
SEE PROFILE

Michael W Parker
Saint Vincent's Institute
346 PUBLICATIONS **12,425** CITATIONS
SEE PROFILE

Published in final edited form as:
J Mol Biol. 2007 April 13; 367(5): 1227–1236. doi:10.1016/j.jmb.2007.01.042.

Structures of Perfringolysin O Suggest a Pathway for Activation of Cholesterol-dependent Cytolysins

Jamie Rossjohn[1,†], **Galina Polekhina**[1,†], **Susanne C. Feil**[1], **Craig J. Morton**[1], **Rodney K. Tweten**[2], and **Michael W. Parker**[1,*]

[1]Biota Structural Biology Laboratory, St. Vincent's Institute of Medical Research, 9 Princes St, Fitzroy, Victoria 3065, Australia

[2]Department of Microbiology and Immunology, The University of Oklahoma Health Sciences Center, Oklahoma City, OK 73190, USA

Abstract

Cholesterol-dependent cytolysins (CDCs), a large family of bacterial toxins, are secreted as water-soluble monomers and yet are capable of generating oligomeric pores in membranes. Previous work has demonstrated that large scale structural rearrangements occur during this transition but the detailed mechanism by which these changes take place remains a puzzle. Despite evidence of structural and functional couplings between domains 3 and 4, the crystal structure of the CDC, perfringolysin O (PFO), shows the two domains do not make direct contact. Here, we present crystal structures of PFO that demonstrate movements of domain 4 are sufficient to trigger conformational changes that are transmitted through the molecule to the distant domain 3. These coupled movements result in a loss of many contacts between domain 3 and rest of the molecule that would eventually lead to the exposure of transmembrane regions in preparation for membrane insertion. The structures reveal a detailed molecular pathway that may be the basis for the allosteric transition that occurs on initial membrane binding leading to the exposure of membrane-spanning regions in a domain distant from the initial site of interaction.

Keywords

cholesterol-dependent cytolysins; membrane insertion; perfringolysin O; pore-forming toxin; X-ray crystallography

The cholesterol-dependent cytolysins (CDCs) are one of the most widely distributed toxins known, having been identified in five different genera of Gram-positive bacteria.[1] The CDCs exhibit a number of unique features amongst pore-forming toxins, including an absolute dependence on the presence of cholesterol-rich membranes for their activity and the formation of very large oligomeric transmembrane pores greater than 150 Å in diameter. More than 20 members of the CDC family have been identified and, for those sequenced, there is a high degree of sequence similarity (40–80% pairwise identities) suggesting they all have similar activities and three-dimensional structures. The three-dimensional atomic

[*]*Corresponding author*mparker@svi.edu.au.
[†]J.R. and G.P. contributed equally to this work.
Present address: J. Rossjohn, Department of Biochemistry and Molecular Biology, School of Biomedical Sciences, Faculty of Medicine, Monash University, Clayton, Victoria 3168, Australia.

Protein Data Bank accession numbers The models have been deposited in the Protein Data Bank§ under the filenames 1PFO (crystal form I) and 1M3I (crystal form III).

structures of two CDCs, perfringolysin O (PFO) from *Clostridium perfringens* and intermedilysin from *Streptococcus intermedius*, have been determined by X-ray crystallography.[2,3] The crystal structures reveal that CDCs are elongated rod-shaped molecules rich in β-sheet and composed of four domains (Figure 1(a)).

Before the crystal structure determination of PFO it was known that a tryptophan-rich region near the C terminus interacted with membranes.[4,5] This region was found to correspond to a loop in domain 4 of the crystal structure (Figure 1(a)). However, the loop was not long enough to span a cell membrane, so it remained a puzzle as to how the toxin formed membrane pores. A major advance in understanding the mechanism of CDC membrane insertion came with the discovery that domain 3 also harbored regions that interact with membranes.[6–8] Studies by Shepard *et al.*[7] and by Shatursky *et al.*[8] revealed that a series of small helices on either side of a central β-sheet could unfurl into β-hairpins, transmembrane hairpin region 1 (TMH1) and transmembrane hairpin region 2 (TMH2), that were capable of spanning membrane bilayers (Figure 1(a)). Such conformational changes were unprecedented amongst bacterial toxins and hence represented a new paradigm for how poreforming proteins interact with membranes.

PFO has been shown to oligomerize on the membrane surface to form a prepore intermediate before the oligomer inserts into the membrane to form the pore.[9–12] A 40 Å vertical collapse of the PFO molecule, revealed by atomic force microscopy, occurs during the prepore-to-pore transition and was predicted to occur as a result of the structural collapse of domain 2.[13] Saibil and co-workers have recently presented cryoEM structures of the prepore and pore forms of a CDC pore by docking and modeling the PFO structure into images derived from cryo-electron microscopy of pneumolysin.[14,15] Their modeling suggests that domain 4 undergoes a large rotation and twisting relative to domain 2 in the prepore state. The transformation to the pore state is accompanied by domains 3 and 4 undergoing marked rotations with respect to domain 1. As predicted by Czajkowsky and co-workers, the cryoEM data shows that domain 2 completely buckles in the transition causing the molecule to arch over, allowing the TMH regions to approach the membrane surface for insertion.[13]

Key questions of CDC action that remain to be answered include what are the details of the conformational changes that take in the molecule in transiting from the water-soluble to the pore state and what is the trigger that promotes these changes? A number of spectroscopic studies suggest that domain 4 binds to the membrane surface first but does not penetrate deeply. This initial membrane binding triggers an allosteric transition of the toxin monomer that primes it for oligomerization and membrane insertion.[16–19] This domain 4 interaction was found to be a prerequisite for membrane interaction of domain 3, and the domains appeared conformationally coupled. These suggestions have been supported by a study using disulfide-bridged mutants that demonstrated domain 4 interaction with membranes was a prerequisite for domain 3 interactions.[10] Also, domain 3 movement was shown to be a requirement for the unfurling of both β-hairpins TMH1 and TMH2. Despite evidence of structural and functional couplings between domains 3 and 4, the crystal structure of the PFO monomer shows the two domains do not contact each other directly and there is only a single glycine linker between domain 4 and the rest of the molecule (Figure 1(a)).[2]

Here, we present crystal structures of different conformational states of PFO that demonstrate movements of domain 4 are sufficient to trigger conformational changes that are transmitted through the molecule to the distant domain 3. These movements result in a loss of many contacts between domain 3 and the rest of the molecule that would eventually lead to the exposure of TMH1 to solvent, freeing this region for membrane insertion. The structures explain why initial binding of domain 4 to membranes is a prerequisite for pore

formation and suggest that low pH, a known membrane-inserting trigger for other bacterial toxins, may have a role in the observed allosteric changes.

High-resolution structure of PFO

The structure of PFO has been determined in three different crystal forms, termed I, II and III. Crystal form I, grown from PEG 20000 solutions, contains one PFO monomer per asymmetric unit and represents the crystal form from which the medium-resolution structure was determined.[2] The structure of PFO derived from crystal form II, grown from butanol solutions,[20] is identical with that of crystal form I and is not discussed further.[21] A more accurate structure has been determined from crystal form I on the basis of higher resolution data to 2.2 Å (Table 1). The structure provides a clearer view of the regions within the molecule that have been shown to interact with the membrane, as well as highlighting the role water-mediated contacts have in domain–domain stabilization.

The membrane-inserting regions TMH1 and TMH2 are packed on either side of the central β-sheet in domain 3 (Figure 1(a)). For PFO to enter the membrane, domain 3 has to swing away from the body of the molecule to allow the TMH regions to unwind. TMH1 has to break contacts with the β-sheets of domains 2 and 3 and a region of domain 1, whilst TMH2 has to predominantly peel away from domains 2 and 3. Both TMH regions are involved in a significant number of intramolecular contacts (Figure 2 and Table 2). TMH1 is involved in 16 hydrogen bonding contacts and TMH2 is involved in nine hydrogen bonding contacts. Overall, there are a significant number (ten) of interactions that are water-mediated, and there are many interactions that involve main-chain atoms from the TMH regions (nine in TMH1 and six in TMH2).

Previous studies have indicated that domain 4 is highly flexible.[14,22,23] Domain 4 is connected to domain 2 *via* a single glycine linker and the only contacts with the rest of the molecule involve this domain. The van der Waals interactions at the domain 2/4 interface are centered around Phe75, making contacts with Val413, Tyr415, Ala447 and Asn448 (Figure 3(a)). There is one salt-bridge (between Lys70 and Glu412/Glu446) and one hydrogen bond between main-chain atoms of Asn73 and Lys391. In addition, there are water-mediated hydrogen bonds between main-chain atoms of Tyr415, Asp416 and Lys66; Arg450, Tyr415 and Tyr389; Lys66 and Glu421 (Figure 3(a)). In total, there is one salt-bridge and six polar interactions between the two domains.

Structure of PFO in crystal form III

Crystal form III was grown using PEG 8000 at low pH and contains four molecules per asymmetric unit. The structure of PFO in this crystal form, with four molecules in the asymmetric unit, has been solved (Table 1). Although the individual domains, with the exception of domain 2, superimpose closely with the high-resolution crystal form I structure, there are considerable variations in the placement of domains with respect to one another (Figure 1(b)). Superposition of domain 1 of all four molecules in the asymmetric unit of crystal form III with respect to domain 1 of the high-resolution crystal form I structure reveals rotations of domain 4 between 5° and 15°. Similarly, domain 3 rotates between 5° and 8°. The rotations of these two domains appear coupled: the larger the rotation of domain 4, the larger the rotation of domain 3. Domain 2 does not superimpose well between the molecules. This aspect is discussed further below. Comparison of the structure from crystal form I with the molecule exhibiting the largest differences in crystal form III reveals there is no large-scale structural change that occur between domain 2 and domain 4, apart from the loss of a main-chain hydrogen bond between Asn73 and Lys391. The major structural differences arise from loss of contacts in the crystal form III molecule between domain 2 and the base of domain 3, involving residues in the TMH1 and TMH2 regions. Nine

hydrogen bonding interactions are absent from TMH1: Ser188 to Asp380 (water-mediated); Lys189 to Asp58 (water-mediated); Ser194 to Asn377(water-mediated); Leu196 to Tyr278 (water-mediated); Asn205 to Lys332 (water-mediated); Ser206 to Lys332; Asp210 to Glu282 (water-mediated); Asp210 to Lys219; Asn216 to Lys69 (see Figure 2 (a) *versus* (c)). Five hydrogen bonds are absent from TMH2: Ser285 to Glu388 (water-mediated), Ser286 to Ser386 (main-chain), Ser286 to Glu388 (main-chain); Lys288 to Glu388 (water-mediated); Gln291 to Glu183 (water-mediated) (see Figure 2 (b) *versus* (d)). In addition, a van der Waals interaction between Ile76 and Ser286 is lost. The conformation of the Trp-rich loop is very similar to that observed in the other crystal forms but with some variability in the selection of the side-chain rotamers of Leu462, Glu465 and Trp466.

PFO dimers?

The four monomers in crystal form III assemble into two pairs of head-to-tail dimers. Although there is only one monomer in the asymmetric unit in crystal form I, it does form a crystallographic dimer. Intriguingly, this dimer also packs head-to-tail and superimposes reasonably closely to the dimers observed in crystal form III (Figure 1(c)). (A crystallographic dimer in crystal form II is also closely superimposable on the dimers in the other crystal forms (unpublished results)). The major subunit interactions involve domain 3 of one molecule interacting with domain 4 of the other molecule. There is a recent report that PFO can form dimers in solution as monitored by analytical ultracentrifugation and small-angle X-ray scattering.[24] The K_d for the monomer-to-dimer equilibrium was reported to be 0.2 μM, a concentration 100-fold lower than that used to form the crystals described here. In the dimers observed in the crystals, the surface buried at the interface is approximately 450 Å^2 per monomer, a value lower than typical protein–protein interfaces. However, there is a high shape complementarity coefficient of 0.56, reflected by a significant number of contacts between the monomers at the interface, including three salt-bridges, 31 potential hydrogen bonds and 82 van der Waals contacts. It is thus plausible that PFO head-to-tail dimers do exist at high concentrations of protein but would require dissociation to form the parallel dimers seen in the prepore and pore forms of the toxin.[25]

Domain flexibility

The medium-resolution crystal structure of PFO suggested both domains 3 and 4 might be highly flexible,[2] and this suggestion has been supported by viscometry studies,[22] neutron scattering[23] and, more recently, electron microscopy studies.[14,15] In domain 3, the core β-sheet that runs through domains 1 and 3 has a highly pronounced curvature at the domain interface (Figure 1(a)). The packing of domain 3 onto domain 2 is far from complementary and consists of predominantly polar contacts. Both features were compatible with suggested flexing of domain 3 away from the body of the molecule in order to relieve stress at the domain 1–3 interface.[2] The discovery that domain 3 harbored membrane-interacting regions of the toxin[7,8] indicated that domain 3 flexing was more than a mechanism of relieving stress but was an essential step in membrane insertion. This is because one of the membrane-spanning regions, TMH1, is buried in the domain 1–2 interface, and hence flexing of domain 3 is critical to release TMH1 from the body of the molecule for membrane insertion. The crystal structures reported here demonstrate directly that both domains 3 and 4 are flexible domains but domain 2 is the most flexible part of the molecule. It has been proposed by others that this domain collapses on formation of the pore (see below). A translational/librational/screw (TLS) motion determination analysis‡ of both crystal forms demonstrates that the PFO molecule can be considered in terms of four flexible rigid bodies: domains 1+3, TMH2, domain 2, and domain 4.[26,27]

Coupled rotation of domains

The crystal structures reported here demonstrate that significant domain movements can occur even in the restricted environment of a crystal lattice. Comparison of the structures of each independent molecule in crystal form III shows that domain 4 rotations are coupled to domain 3 rotations, and provides a detailed atomic description of how the movements are coupled despite the fact that there is no direct interaction between the two domains. Such a coupled movement of these domains in all four monomers indicates that the observed movements are inherent to the molecule rather than being an artifact of crystal lattice forces. The crystallographic results provide views of PFO in which domain 4 rotations of more than 15° are observed (Figure 1(b)). Although there is only one covalent connection between domains 2 and 4, there are relatively few changes in the non-covalent contacts between them on rotation. The fulcrum about which the rotation occurs is located in the middle of the β-sheet in domain 2 rather than at the domain linker. As described above, the domain 2–4 interface is predominantly hydrophobic in nature and is the only such interface in the toxin. Thus, although there is only one covalent connection between domain 4 and the rest of the molecule, the interfacial interactions are sufficiently strong to inhibit domain rotation about the linker. Rotation of domain 4 is accompanied by considerable flexing of the β-sheet in domain 2 leading to a large loss of contacts (including nine hydrogen bonds) between domain 2 and the tip of domain 3 (near the TMH regions) (Figure 2). This weakening of the domain 2–3 interface correlates with the rigid body rotation of domain 3 away from domain 1. These observations lead to the conclusion that sufficient rotation of domain 4 could destroy all the contacts at the domain 2–3 interface. This would provide a mechanism for relieving the stress of the highly bent β-sheet core of domains 1 and 3 by allowing a coupled rotation of domain 3 away from the body of the molecule. The domain 3 rotation would then enable the release of the TMH regions for membrane insertion.

Deformation of domain 2

Czajkowsky and co-workers, using atomic force microscopy, first showed that upon prepore to pore conversion a large vertical collapse occurs in the oligomeric complex of PFO.[13] This collapse was measured also by FRET between probes within the structure of PFO and the membrane surface.[28] Saibil and co-workers subsequently reached a similar conclusion based on modeling of the PFO structure into cryo-electron microscopy images of pneumolysin in both the prepore and pore states.[15] Furthermore, it was hypothesized that it is the membrane insertion step that causes changes in the domain 2–4 interface leading to deformation of domain 2.[15,29]

There is some evidence of distortion of domain 2 in the crystal structures presented here. Domain 2 does not superimpose well between molecules of crystal forms I and III (Figure 3(b)). There is a hinge-bending motion at the domain 1–2 interface and a twist of the β-sheet about the middle of domain 2 as defined by an axis running through Val64, Arg80 and Thr384. These residues are located where there is already a marked twist in the domain 2 β-sheet caused by a β-bulge (residues 59–63). The amount of distortion also appears coupled to the amount of rotation domain 4 experiences relative to the crystal form I structure (Figure 1(b) *versus* Figure 3(b)). Thus, structural alterations in domain 2 are likely to start occurring before the membrane insertion step, since further domain 4 movements are observed in the prepore compared to the crystal structures presented here.[15]

Role of the Trp-rich loop

The Trp-rich loop has been hypothesized to spring out from the body of domain 4 on binding of cholesterol.[2] Thus, cholesterol binding could be the trigger for the transmission of conformational changes that lead to eventual release of domain 3. However, in the

structures reported here, the Trp-rich loop is superimposable despite the loosening of the domain 2–3 interface. Recent work shows that, although cholesterol may be involved in the initial membrane-binding event of some CDCs, the sterol is essential for the conversion of prepore to pore.[29] In the CDC toxin intermedilysin, the Trp-rich loop has been shown not to be involved in membrane binding but is essential for the prepore-to-pore conversion.[3] Thus, movements of the loop do not appear important for the initial loosening of domain 3 from the body of the molecule but it cannot be ruled out that it has a role in the final release of domain 3 before membrane insertion.

A low pH trigger?

A number of bacterial toxins are known to preferentially insert into lipid membranes at low pH.[30] Low pH may help the initial electrostatic steering towards the membrane surface and in doing so promote the correct orientation of the toxin molecule for membrane insertion. In the case of diphtheria toxin, low pH is thought to neutralise acidic loops, rendering them more hydrophobic and lowering the energy costs of membrane insertion.[31] For some toxins, low pH promotes the transition of the protein from its native state to a molten globule state and hence lowering the energy barrier of conversion from the water-soluble state to membrane inserted state. One CDC family member, listeriolysin O, has been reported to have a pronounced acidic pH optimum for activity[32] and PFO is more active at lower pH.[33]

The cause of the coupled domain movements observed in the PFO crystal structures could be ascribed to crystal packing forces, since both domains 3 and 4 are involved in crystal contacts in each of the four monomers that pack within the asymmetric unit. Alternatively, the movements may be due to low pH (crystal forms I and II grow at pH values above 7,[20] whereas crystal form III grows at pH 5.4) or some combination of crystal forces and low pH. Comparison of the structure of each independent molecule in this crystal form shows that domain 4 rotations are coupled to domain 3 rotations. There are three interactions between the domain interfaces of the crystal form I structure that are absent from the crystal form III structure that might be affected by low pH: Asp58, Asp380 and Glu388 all form interactions that bridge domain 2 to TMH1 and TMH2 of domain 3 (Figure 2). These interactions are absent from crystal form III and it is plausible that the pK_a of one or more of these residues may be raised by its microenvironment sufficiently that their interactions are susceptible to breakage in a low-pH environment. Theoretical calculations predict that Asp58 would have a sufficiently high pK_a value of 5.95, consistent with this hypothesis.[34]

It has been argued that the pH at the surface of membranes that possess some net negative local charge (for example, due to anionic phospholipids in prokaryotic cells or glycosylated membrane proteins in eukaryotic cells) is much lower than that of the bulk solvent.[35] Hence, it is possible that although PFO can work at neutral pH, the lower pH at the membrane surface is sufficient to trigger the conformational changes observed here. It is possible also that the apparent low-pH effect we see with the crystal structures is reflecting some alternative *in vivo* trigger such as binding to cholesterol molecules. These ideas correlate well with the orginal suggestions of Bhakdi and co-workers that CDCs are activated allosterically by the target membrane.[16,17]

Concluding remarks

The structures presented here suggest how initial interaction with membranes *via* domain 4 is allosterically transmitted to the distant domain 3. The formation and breakage of contacts between domains 2 and 3 is at the very heart of CDC activity. Premature firing of the TMH regions in domain 3 of a CDC must be avoided in order for the host bacterium's toxin to successfully cause cell lysis. Premature firing would risk either aggregation or non-productive association with the membrane surface. The firing of the β-hairpins is regulated

by rotation of domain 3, which, in turn, is dependent on the breakage of contacts at the domain 2–3 interface. The structures reported here show that these contacts can be formed or broken depending on the rotational state of domain 4 with respect to the long axis of the molecule.

Acknowledgments

This work was supported by a grant from the National Health and Medical Research Council of Australia (NHMRC) to M.W.P. J.R. was supported by a Wellcome Trust Senior Research Fellowship in Biomedical Sciences in Australia, G.P. was supported by an NHMRC RD Wright Fellowship and M.W.P. was supported by an NHMRC Senior Principal Research Fellowship.

Abbreviations used

CDCs	cholesterol-dependent cytolysins
TMH	transmembrane hairpin regions
PFO	perfringolysin O

References

1. Tweten RK, Parker MW, Johnson AE. The cholesterol-dependent cytolysins. Curr. Top. Microbiol. Immunol. 2001; 257:15–33. [PubMed: 11417120]
2. Rossjohn J, Feil SC, McKinstry WJ, Tweten RK, Parker MW. Structure of a cholesterol-binding, thiol-activated cytolysin and a model of its membrane form. Cell. 1997; 89:685–692. [PubMed: 9182756]
3. Polekhina G, Giddings KS, Tweten RK, Parker MW. Insights into the action of the superfamily of cholesterol-dependent cytolysins from studies of intermedilysin. Proc. Natl Acad. Sci. USA. 2005; 102:600–605. [PubMed: 15637162]
4. Nakamura M, Sekino N, Iwamoto M, Ohno-Iwashita Y. Interaction of θ-toxin (perfringolysin O), a cholesterol-binding cytolysin, with liposomal membranes: change in the aromatic side chains upon binding and insertion. Biochemistry. 1995; 34:6513–6520. [PubMed: 7756282]
5. Sekino-Suzuki N, Nakamura M, Mitsui KI, Ohno-Iwashita Y. Contribution of individual tryptophan residues to the structure and activity of θ-toxin (perfringolysin-O), a cholesterol-binding cytolysin. Eur. J. Biochem. 1996; 241:941–947. [PubMed: 8944786]
6. Palmer M, Saweljew P, Vulicevic I, Valeva A, Kehoe M, Bhakdi S. Membrane-penetrating domain of streptolysin O identified by cysteine scanning mutagenesis. J. Biol. Chem. 1996; 271:26662–26667.
7. Shepard LA, Heuck AP, Hamman BD, Rossjohn J, Parker MW, Ryan KR, et al. Identification of a membrane-spanning domain of the thiol-activated pore-forming toxin *Clostridium perfringens* perfringolysin O: an alpha-helical to beta-sheet transition identified by fluorescence spectroscopy. Biochemistry. 1998; 37:14563–14574. [PubMed: 9772185]
8. Shatursky O, Heuck AP, Shepard LA, Rossjohn J, Parker MW, Johnson AE, Tweten RK. The mechanism of membrane insertion for a cholesterol-dependent cytolysin: a novel paradigm for poreforming toxins. Cell. 1999; 99:293–299. [PubMed: 10555145]
9. Shepard LA, Shatursky O, Johnson AE, Tweten RK. The mechanism of pore assembly for a cholesterol-dependent cytolysin: formation of a large prepore complex precedes the insertion of the transmembrane beta-hairpins. Biochemistry. 2000; 39:10284–10293. [PubMed: 10956018]
10. Hotze EM, Wilson-Kubalek EM, Rossjohn J, Parker MW, Johnson AE, Tweten RK. Arresting pore formation of a cholesterol-dependent cytolysin by disulfide trapping synchronizes the insertion of the transmembrane beta-sheet from a prepore intermediate. J. Biol. Chem. 2001; 276:8261–8268. [PubMed: 11102453]
11. Hotze EM, Heuck AP, Czajkowsky DM, Shao Z, Johnson AE, Tweten RK. Monomer-monomer interactions drive the prepore to pore conversion of a beta-barrel-forming cholesterol-dependent cytolysin. J. Biol. Chem. 2002; 277:11597–11605. [PubMed: 11799121]

12. Heuck AP, Tweten RK, Johnson AE. Beta-barrel pore-forming toxins: intriguing dimorphic proteins. Biochemistry. 2001; 40:9065–9073. [PubMed: 11478872]
13. Czajkowsky DM, Hotze EM, Shao Z, Tweten RK. Vertical collapse of a cytolysin prepore moves its transmembrane β-hairpins to the membrane. EMBO J. 2004; 23:3206–3215. [PubMed: 15297878]
14. Gilbert RJC, Jimenez JL, Chen S, Tickle IJ, Rossjohn J, Parker MW, et al. Two structural transitions in membrane pore formation by pneumolysin, the pore-forming toxin of *Streptococcus pneumoniae*. Cell. 1999; 97:647–655. [PubMed: 10367893]
15. Tilley SJ, Orlova EV, Gilbert RJC, Andrew PW, Saibil HR. Structural basis of pore formation by the bacterial toxin pneumolysin. Cell. 2005; 121:247–256. [PubMed: 15851031]
16. Palmer M, Vulicevic I, Saweljew P, Valeva A, Kehoe M, Bhakdi S. Streptolysin O: a proposed model of allosteric interaction between a pore-forming protein and its target lipid bilayer. Biochemistry. 1998; 37:2378–2383. [PubMed: 9485385]
17. Abdel Ghani EM, Weis S, Walev I, Kehoe M, Bhakdi S, Palmer M. Streptolysin O: inhibition of the conformational change during membrane binding of the monomer prevents oligomerization and pore formation. Biochemistry. 1999; 38:15204–15211. [PubMed: 10563803]
18. Heuck AP, Hotze EM, Tweten RK, Johnson AE. Mechanism of membrane insertion of a multimeric beta-barrel protein: perfringolysin O creates a pore using ordered and coupled conformational changes. Mol. Cell. 2000; 6:1233–1242. [PubMed: 11106760]
19. Ramachandran R, Heuck AP, Tweten RK, Johnson AE. Structural insights into the membrane-anchoring mechanism of a cholesterol-dependent cytolysin. Nature Struct. Biol. 2002; 11:823–827. [PubMed: 12368903]
20. Feil SC, Rossjohn J, Rhode K, Tweten RK, Parker MW. Crystallization and preliminary X-ray analysis of a thiol-activated cytolysin. FEBS Letters. 1996; 397:290–292. [PubMed: 8955365]
21. Polekhina, G.; Feil, SC.; Tang, J.; Rossjohn, J.; Giddings, KS.; Tweten, RK.; Parker, MW. Comparative three-dimensional structure of cholesterol-dependent cytolysins. In: Alouf, JE.; Popoff, MR., editors. The Comprehensive Sourcebook of Bacterial Protein Toxins. 3rd edit. Elsevier; London: 2006. p. 659-670.
22. Morgan PJ, Hyman SC, Byron O, Andrew PW, Mitchell TJ, Rowe AJ. Modeling the bacterial protein toxin, pneumolysin, in its monomeric and oligomeric form. J. Biol. Chem. 1994; 269:25315–25320. [PubMed: 7929224]
23. Gilbert RJC, Rossjohn J, Parker MW, Tweten RK, Morgan PJ, Mitchell TJ, et al. Self-interaction of pneumolysin, the pore-forming protein toxin of *Streptococcus pneumoniae*. J. Mol. Biol. 1998; 284:1223–1237. [PubMed: 9837740]
24. Solovyova AS, Nöllmann M, Mitchell TJ, Byron O. The solution structure and oligomerization behavior of two bacterial toxins: pneumolysin and perfringolysin O. Biophys. J. 2004; 87:540–552. [PubMed: 15240487]
25. Gilbert RJC. Inactivation and activity of cholesterol-dependent cytolysins: what structural studies tell us. Structure. 2005; 13:1097–1106. [PubMed: 16084382]
26. Painter J, Merritt EA. TLSMD web server for the generation of multi-group TLS models. J. Appl. Crystallog. 2006; 39:109–111.
27. Painter J, Merritt EA. Optimal description of a protein structure in terms of multiple groups undergoing TLS motion. Acta Crystallog. sect D. 2006; 62:439–450.
28. Ramachandran R, Tweten RK, Johnson AE. The domains of a cholesterol-dependent cytolysin undergo a major FRET-detected rearrangement during pore formation. Proc. Natl Acad. USA. 2005; 102:7139–7144.
29. Giddings KS, Johnson AE, Tweten RK. Redefining cholesterol's role in the mechanism of the cholesterol-dependent cytolysins. Proc. Natl Acad. Sci. USA. 2003; 100:11315–11320. [PubMed: 14500900]
30. Parker MW, Pattus F. Rendering a membrane protein soluble in water: a common packing motif in bacterial protein toxins. Trends Biochem. Sci. 1993; 18:391–395. [PubMed: 8256289]
31. Choe S, Bennett MJ, Fujii G, Curmi PM, Kantardjieff KA, Collier RJ, Eisenberg D. The crystal structure of diphtheria toxin. Nature. 1992; 357:216–222. [PubMed: 1589020]

32. Glomski IJ, Gedde MM, Tsang AW, Swanson JA, Portnoy DA. The *Listeria monocytogenes* hemolysin has an acidic pH optimum to compartmentalize activity and prevent damage to infected cells. J. Cell Biol. 2002; 156:1029–1038. [PubMed: 11901168]
33. Portnoy DA, Tweten RK, Kehoe M, Bielecki J. Capacity of listeriolysin O, streptolysin O, and perfringolysin O to mediate growth of *Bacillus subtilis* within mammalian cells. Infect. Immun. 1992; 60:2710–2717. [PubMed: 1612739]
34. Yang AS, Gunner MR, Sampogna R, Sharp K, Honig B. On the calculation of pKas in proteins. Proteins: Struct. Funct. Genet. 1993; 15:252–265. [PubMed: 7681210]
35. van der Goot FG, González-Mañas JM, Lakey JH, Pattus F. A 'molten-globule' membraneinsertion intermediate of the pore-forming domain of colicin A. Nature. 1991; 354:408–410. [PubMed: 1956406]
36. Kraulis P. MOLSCRIPT: a program to produce both detailed and schematic plots of proteins. J. Appl. Crystallog. 1991; 24:946–950.
37. Otwinowski Z, Minor W. Processing of X-ray diffraction data collected in the oscillation mode. Methods Enzymol. 1997; 276:307–326.
38. Brünger, AT. XPLOR: A System for X-ray Crystallography and NMR. Yale University; New Haven, CT: 1993.
39. Brünger AT, Adams PD, Clore GM, DeLano WL, Gros P, Grosse-Kunstleve RW, et al. Crystallography & NMR system: a new software suite for macromolecular structure determination. Acta Crystallog. sect D. 1998; 54:905–921.
40. Laskowski RA, McArthur MW, Moss DS, Thornton JM. PROCHECK: a program to check the stereochemical quality of protein structures. J. Appl. Crystallog. 1993; 26:282–291.
41. Yeates TO. Detecting and overcoming crystal twinning. Methods Enzymol. 1997; 276:344–358. [PubMed: 9048378]
42. 4., Collaborative Computational Project Number. The CCP4 suite: programs for protein crystallography. Acta Crystallog. sect D. 1994; 50:750–763.

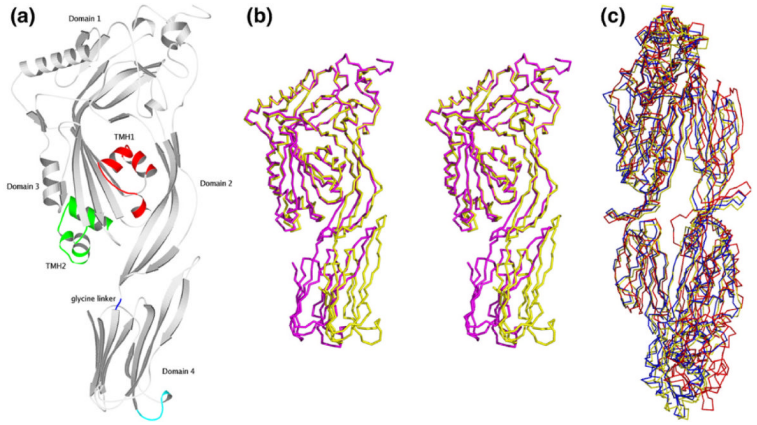

Figure 1.

Three-dimensional structure of perfringolysin O. (a) A ribbon picture of PFO showing the Trp-rich loop in domain 4 cyan, the glycine linker between domains 2 and 4 in dark blue and the membrane interacting regions TMH1 and TMH2 in red and green, respectively. (b) Superposition of PFO from different crystal forms. Shown is PFO from crystal form I (magenta) and monomer A of crystal form III (yellow), highlighting the movement in domain 4. The monomers were superimposed based on domain 1. (c) Superposition of PFO dimers. Crystal form I is in yellow, the AC dimer of crystal form III is in red and the BD dimer of crystal form III is in blue. This and the following Figures were produced using MOLSCRIPT[36] or PyMOL [http://pymol.sourceforge.net/].

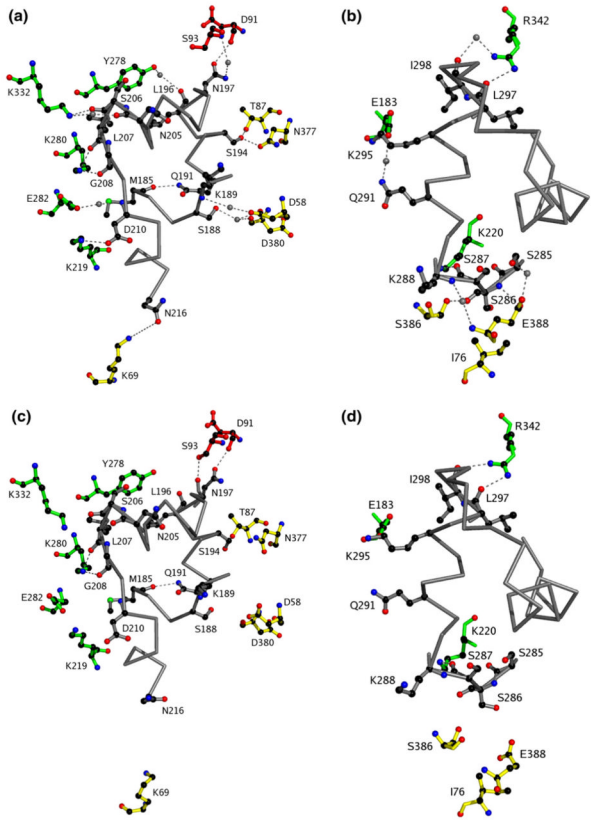

Figure 2.

Views of the membrane-interacting regions of domain 3 in different crystal forms. The regions surrounding TMH1 and TMH2, as seen in the high-resolution structure of PFO determined from crystal form 1 and in one of the monomers of crystal form III. The TMH regions are highlighted in gray. Water molecules are depicted as gray spheres. Polar interactions are denoted by broken lines. Residues from domains 1, 2 and 3 are in shown in red, yellow and green, respectively. (a) TMH1 in crystal form I; (b) TMH2 in crystal form I; (c) TMH1 in crystal form III; (d) TMH2 in crystal form III.

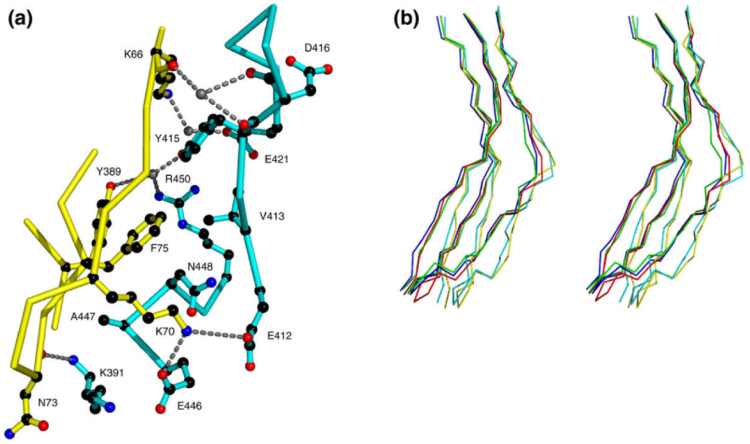

Figure 3.
View of domain 2 in the different crystal forms. (a) View of the domain 2 – domain 4 interface. Residues from domains 2 and 4 are in shown in yellow and blue bonds, respectively. (b) Superposition of domain 2 of PFO from different crystal forms. Crystal form I is in blue and the four molecules of crystal form III are shown in yellow, green, cyan and red.

Table 1

Crystallographic data and refinement statistics

A. *Data collection statistics*		
Crystal form	I	III
Temperature (K)	100	100
X-ray source[a]	Photon Factory	In-house
Space group	$C222_1$	$P3_1$
Cell dimensions (Å)		
a (Å)	47.0	130.4
b (Å)	178.0	130.4
c (Å)	174.2	129.9
Resolution (Å)	2.2	2.9
No. observations	108,275	148,733
No. unique reflns	32,396	59,700
Multiplicity	3.3	2.5
Data completeness (%)	85.7 (88.0)	97.8 (97.4)
No. data $>2\sigma_I$	73.4 (50.4)	73.4 (38.5)
I/σ_I	20.7 (4.9)	16.8 (1.8)
R_{merge} (%)	5.5 (26.1)	6.1 (57.1)
B. *Refinement statistics*		
Non-hydrogen atoms		
Protein	3705	14,628
Water	330	306
Resolution (Å)	2.2	2.9
R_{factor} (%)	21.1	23.3
R_{free} (%)	26.8	29.9
rms deviations from ideality		
Bond lengths (Å)	0.007	0.006
Bond angles (deg.)	1.5	1.1
Impropers (deg.)	0.7	0.6
Dihedrals (deg.)	28.0	26.5
Residues in most favored region of Ramachandran plot (%)	99.8	99.6
Average *B*-factors (Å^2)		
Main chain	44.9	68.0
Side-chain	46.4	68.7
Water	47.4	47.7
r.m.s deviation bonded *B*-factors	2.7	4.3

Notes PFO was over-expressed and purified as described.[20] Both crystal forms were grown using the hanging-drop, vapor-diffusion technique at room temperature. The procedure for growing crystal form I was as described.[20] Crystal form III grow as long hexagonal rods in 100 mM Mes (pH 5.4) and using 8% (w/v) PEG 8000 as the precipitant and a protein concentration of 10 mg/ml in 10 mM Hepes (pH 7.5), 1 mM DTT. The crystals grow at room temperature and take about a week to reach final size. All crystals were flash-frozen. The diffraction data were processed using DENZO and SCALEPACK.[37] The structures were refined using similar protocols, with either X-PLOR[38] or CNS.[39] Tightly-restrained

individual *B*-factor refinement was used and bulk solvent corrections were applied to all data sets. In cases where there was more than one molecule in the asymmetric unit, non-crystallographic symmetry restraints were applied. The structure of PFO was determined originally from crystal form I using 2.7 Å resolution X-ray data collected at room temperature. A high-resolution data set was collected on the 6A2 beamline of the Photon Factory (Tsukuba, Japan) from a flash-frozen crystal. To avoid unacceptably high mosaicity, the crystals had to be transferred from 5% to 20% (v/v) MPD, with a soak for 30 minutes for each 5% increment. The crystals were indexed in space group $C222_1$ with unit cell dimensions a=47.0 Å, b=178.0 Å and c=174.2 Å. Notably, the b cell edge had shrunk by 4 Å compared to the previous room temperature data set.[20] The starting model for the refinement was the medium-resolution structure after omitting water molecules. Rigid body refinement was used initially, followed by a number of iterative rounds of simulated annealing refinement and model building. The final model includes all residues (30 to 500; the first 20 residues constitute the signal peptide that was cleaved from the construct) and 330 water molecules. Although the first nine residues have very high *B*-factors (>80 $Å^2$), there was clear electron density for them and their inclusion lowered the R_{free} value. All residues lie within the allowed regions of the Ramachandran plot with only one residue in the generously allowed region.[40] This residue, Ile31, is located at the mobile N terminus and hence its placement is uncertain. The high-resolution structure superposes closely with the published structure with an overall r.m.s. deviation of 0.4 Å for all C^{α} atoms. The major outliers (>1.5 Å) fall between residues 56 and 61. This is a region of relatively poor electron density that reflects local disorder within the structure. The model includes seven residues at the N terminus that were not observed in the 2.7 Å resolution published structure.[2]

Crystal form III was initially assigned to space group $P6_2$ with unit cell dimensions $a=b$=130.4 Å, c=129.9 Å. The crystals diffracted very strongly to the water ring, but did not diffract much beyond this limit, suggesting a degree of disorder within the crystals. Subsequently, it was realized that the crystals were heavily twinned merohedrally with a twinning fraction greater than 0.4.[41] The data were subsequently reprocessed in space group $P3_1$ and detwinned using CCP4 programs.[42] The new space group was consistent with up to four molecules in the asymmetric unit. Molecular replacement attempts using the high-resolution model from crystal form I failed. However, a search model comprising only domains 1, 2 and 3 yielded two convincing solutions in the translation function, although superposing the intact molecule resulted in clashes involving domain 4. Domain 4 was then used as a search probe, after fixing the positions of the other domains based on the initial molecular replacement solution. Given the low signal expected from using such a search probe, normalized structure factors were used. Two rotation function peaks, listed 27th and 28th in the peak list, gave peaks in the translation function that were significantly above the noise level (correlation coefficients of 0.28 and 0.23, respectively, against a noise level of 0.19). Rigid body fitting of the four solutions resulted in a correlation coefficient of 0.39, and an R_{factor} of 41%. Surprisingly, the two domain 4 solutions did not relate to the two identified domain 1–3 solutions, and hence represented two independent PFO molecules within the asymmetric unit. Thus, it seemed there were four partial models within the asymmetric unit, two encompassing domains 1–3 only (molecules A and B) and two comprising domain 4 only (molecules C and D). Map calculations using the rigid-body refined partial model revealed unbiased density for domain 4 for molecules A and B. Because of the high twin fraction of the data set being used, further data sets were collected from a number of crystals in an effort to obtain one where there was less of a problem. From about 30 crystals, a complete data set from one crystal was collected where the twin fraction was negligible (0.02). The structure was solved and refined using this data set. The unbiased density for domain 4 from molecules A and B was clearly visible in this data set also. Subsequent maps revealed density that enabled fitting of domains 1–3 of molecules C and D. During energy minimization, the four independent molecules were refined with NCS restraints over individual domains, (excluding domain 2). However, no NCS restraint was used during temperature factor refinement, as the electron density suggested the same domain in each molecule exhibited very different temperature factors.

The values in parentheses are for the highest resolution bin (approximate interval of 0.1 Å). $R_{merge} = \sum_{hkl} \sum_i |I_i - \langle I \rangle| / \langle I \rangle|$, where I_i is the intensity for the ith measurement of an equivalent reflection with indices h,k,l.

[a]Photon Factory is the Weissenberg camera at beamline 6A2, Photon Factory, Tsukuba, Japan. In-house is an MARResearch detector (Hamburg, Germany) on an in-house Rikagu RU-200 rotating anode X-ray generator.

Table 2

Hydrogen bonding contacts of TMH1 and TMH2

A. *TMH1*	
Ser188 –	Asp58
	Asp380 (water-mediated)
Lys189 –	Asp58 (water-mediated)
Gln191 –	Met185
Ser194 –	Th87
	Asn377
Leu 196 –	Tyr278 (water-mediated)
Asn 197 –	Asp91
	Ser93 (water-mediated)
Asn 205 –	Lys332 (water-mediated)
Ser 206 –	Lys332
Leu 207 –	Gly208
	Lys280
Asp 210 –	Lys219
	Glu282 (water-mediated)
Asn 216 –	Lys69
B. *TMH2*	
Ser285 –	Glu388 (water-mediated)
Ser286 –	Ser386
	Glu388
Ser287 –	Lys220
Lys288 –	Glu388 (water-mediated)
Gln291 –	Glu183 (water-mediated)
Lys295 –	Glu183
Leu297 –	Arg342
Ile298 –	Arg342 (water-mediated)